Journal of Electroceramics 2:1, 7–20, 1998

The Dopant Distribution in Ti-, Zr- and Cr-doped $Y_3Al_5O_{12}$ Fibers Grown by the Laser Heated Floating Zone Method

T. KOTANI

Crystal Physics and Electroceramics Laboratory, Department of Materials Science and Engineering, Massachusetts Institute of Technology, Cambridge, MA 02139 USA

Permanent address: Basic High-Technology Laboratories, Sumitomo Electric Industries Ltd., 1-1-3 Shimaya, Konohana-ku, Osaka 554, Japan

J.K.W. CHEN

Crystal Physics and Electroceramics Laboratory, Department of Materials Science and Engineering, Massachusetts Institute of Technology, Cambridge, MA 02139 USA

Permanent address: Form Factor, Inc., 2130 Research Dr., Livermore, CA 94550, USA

H.L. TULLER

Crystal Physics and Electroceramics Laboratory, Department of Materials Science and Engineering, Massachusetts Institute of Technology, Cambridge, MA 02139 USA

Received July 18, 1996; Revised May 19, 1997; Accepted July 31, 1997

Abstract. Single crystal fibers of Ti-, Zr- and Cr-doped $Y_3Al_5O_{12}$ (YAG) were grown from polycrystalline feed rods in $Ar + 5\%H_2$, pure Ar and $Ar + 2\%O_2$ atmospheres using the laser heated floating zone method. The spatial dopant distribution and precipitation of second phases in the grown fibers has been systematically studied by means of electron probe microanalysis. A strong growth-atmosphere dependence of effective segregation coefficient and precipitate formation were seen in Ti- and Cr-doped fibers, but not in Zr-doped fibers. The highest doping of Ti into the YAG lattice was obtained in $Ar + 5\%H_2$ atmosphere, while Cr was able to be incorporated into YAG by suppression of evaporation under an $Ar + 2\%O_2$ atmosphere. The results are discussed in terms of atmosphere-dependent valence state and volatility of the dopant.

Keywords: crystal growth, $Y_3Al_5O_{15}$, YAG, optical fibers

1. Introduction

YAG is a well-known laser host material with a flexible structure which can accommodate a diversity of dopants. This has led to many studies of YAG doped with a wide variety of metal elements both to clarify dopant-property correlations and to identify new laser materials [1–6]. A number of techniques including Czochralski [4–6], Bridgman [7,8] and floating zone [9] have been employed in an attempt to grow crystals of high quality and controlled impurity concentrations and distributions. In any growth method, effective segregation coefficients and dopant solubilities are fundamental information for the purpose of growing crystals with well-defined doping levels since most dopants have non-unity segregation coefficients and limited solubilities [10]. Further, the dopant re-distribution and solubility often depend strongly on growth atmosphere, especially for multivalent metal elements [11]. In this study, we are particularly interested in three dopants, Ti, Cr and Zr since these dopants have a moderate solubility in the YAG lattice and differ in a number of ways including valence state, ionic radius, coordination number and volatility at high temperatures. While some growth studies with these dopants have previously been

reported, there have been no systematic studies on the incorporation of these dopants into YAG under different atmospheres [4–6,13–15].

In recent years, the laser heated floating zone (LHFZ) method for fiber growth has been developed primarily as a materials research tool, particularly for novel laser and refractory materials, and its versatility and advantages have been extensively demonstrated [16–18]. In this study we have taken advantage of some of its special features (see below) and grown a variety of YAG fibers, typically 1 mm in diameter and 5–20 mm long, doped with Ti, Zr and Cr in three different growth atmospheres, $Ar + 5\%H_2$, Ar and $Ar + 2\%O_2$. Quantitative spatial distributions of the dopants and critical dopant concentration for precipitation have been systematically examined by means of electron probe microanalysis (EPMA). This information was used to investigate growth-atmosphere dependence of effective segregation coefficients and precipitation of the dopants.

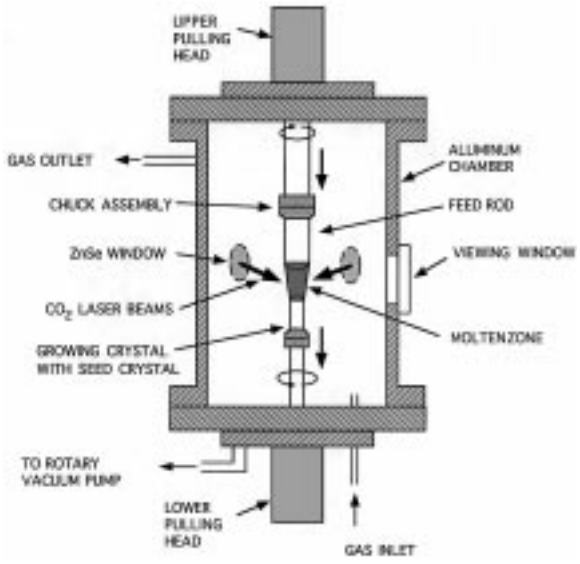

Fig. 1. Schematic diagram of the LHFZ (Laser Heated Floating Zone) growth apparatus.

2. Experimental

2.1. Fiber Growth by LHFZ Method

The LHFZ growth method is a variation of the conventional floating zone method in that a laser is used as a heat source. Laser heating enables one to grow refractory materials over a wide range of controlled atmospheres. In addition, this technique leads to higher purity crystals given the crucible free and cold-wall growth process. Furthermore, extremely steep temperature gradients can be realized near the growth interface, which is preferable for the growth of heavily doped crystals at relatively high speed without inducing constitutional supercooling [10]. A laser heated floating zone growth system equipped with a 2-beam 100 W CO_2 laser, shown in Fig. 1, was employed for the fiber growth. The LHFZ growth systems are described in more detail elsewhere [19,20].

Polycrystalline feed rods were prepared from doped YAG powders made using a modified Pechini process [21]. This process comprises dissolving a metal salt such as $Y(NO_3)_3$ in distilled water and precipitating out $Y(OH_3)_3$ by adding ammonia (NH_4OH). The filtered precipitate was then dissolved in a solution of citric acid and ethylene glycol. The citric acid solutions of Y, Al and dopants were then mixed together in desired ratios. The mixed solution was dried into a resin, and then the resin was calcined at about 900°C in O_2. The average particle size was about 0.5 μm. All the powders were single phase according to X-ray diffraction analysis. The YAG powders were pressed at 400 psi, and then isostatically pressed at 40,000 psi for a few minutes to make pellets. The pellets were then sintered in vacuum at 1800°C for two hours for densification. The density of the obtained pellets ranged from 85–95% of theoretical. According to spectrochemical analysis (ICP-AES: Inductively Coupled Plasma Atomic Emission Spectrometry), actual doping concentrations in the feed rods were equal to the nominal composition within the error (usually a factor of two) associated with spectrochemical analyses.

Nominal composition of the feed rods made in this study are listed in Table 1. The dopant concentrations, expressed as an atomic percent of the doped cation in YAG, were chosen based on the reported solubility. The polycrystalline rods were prepared with square cross sections with dimensions of $\approx 1\,\text{mm} \times \approx 1\,\text{mm} \times \approx 15\,\text{mm}$ and weights of from 60–100 mg. The colors of the feed rods prepared in this study are listed in Table 1. EPMA revealed that the feed rods doped with 0.25at.% Cr, or 0.76at.% and 1.5at.% Zr contained precipitates of Cr_2O_3 or $Y_{0.15}Zr_{0.85}O_{1.93}$, respectively.

Table 1. Normal compositions and color of polycrystalline feed rods employed for fiber growth. The dopant concentrations are expressed as an atomic percent of the doped cation in YAG

Dopant	Composition		Dopant concentration (at.%)	Color
Ti	$Y_3Al_{5(1-x)}Ti_{5x}O_{12}$:	$x = 0.01$	0.25	light gray to brown gray
		$x = 0.05$	1.25	
		$x = 0.1$	2.50	
Zr	$Y_{3(1-x)}Zr_{3x}Al_5O_{12}$:	$x = 0.01$	0.15	reddish brown
		$x = 0.05$	0.75	
		$x = 0.1$	1.50	
Cr	$Y_3Al_{5(1-x)}Cr_{5xO_{12}}$:	$x = 0.01$	0.25	black

A [111] oriented seed crystal, which was undoped or lightly (< 0.03at.%) Ti- or Zr-doped, and feed rod, each supported on goniometers with 2-direction tilting mechanisms and X-Y positioners were carefully aligned such that the axes of rotation coincided with each other. Both the feed rod and seed were rotated counterwise at 16 rpm and 21 rpm, respectively. The feed rod was heated first to make a melt, and then the seed end was contacted to the melt. The positions of the laser beam spots (approximately 1500 μm in diameter) were adjusted to insure uniform heating and a symmetric melt zone. Then, fiber growth was initiated by pulling both the seed and feed rod down at a constant rate. In this study, a relatively high growth rate, 20 mm/h, was used in order to achieve high doping levels, taking advantage of the features of the LHFZ growth technique. During growth, the laser power, typically 30–38 W, was adjusted so as to maintain a constant zone height. Growth conditions of each fiber are summarized in Table 2.

In preliminary growth experiments, instead of the uniformly doped feed rod described in Table 1, a combination of undoped YAG and a dopant such as TiO_2 was employed as feed rods for the purpose of obtaining a rough estimation of dopant distribution and solubility. In this case, a two step procedure was followed. Prior to fiber growth, the doping step was carried out by dissolving a TiO_2 rod into the molten end of the undoped YAG feed rod. The doping concentration was adjusted with the volume of the TiO_2 rod dissolved into the melt. The TiO_2 source was then replaced by the seed crystal as in the first case. In this case, the dopant concentration in the fiber is expected to decrease exponentially with the growth length [10], so that one can readily see the axial dopant profile and/or precipitation over a wide doping level using only the one fiber. On the other hand, the fibers used for the precise analysis of dopant distribution were grown from the feed rods which had been uniformly doped with a definite concentration because the precise control in the initial doping concentration of the melt is usually difficult in the two-step doping process. The diameter of the grown fiber ranged from 0.9–1.3 mm, which corresponds to 70–90% of the feed rod in cross-section. The growths were typically terminated after gradually decreasing the fiber diameter to less than 0.5 mm in order to reduce thermal shock upon separation from the melt. For the purpose of examining the growth interface as well as the dopant concentration in the melt, the termination was carried out by shutting off the laser

Table 2. Summary of growth conditions

Fiber No.	Dopant concentration in feed rod (at.%)	Atmosphere (static, 1atm)	Growth rate v (mm/h)	Fiber diameter $2r$ (mm)	Zone height h (mm)
TY-1A	Ti 0.25	Ar	20	0.9	1.8
TY-1B	Ti 0.25	$Ar + 5\%H_2$	20	0.9	1.5
TY-1C	Ti 0.25	$Ar + 2\%O_2$	20	0.9	2.1
TY-2A	Ti 1.25	Ar	20	0.9	1.9
TY-2B	Ti 1.25	$Ar + 5\%H_2$	20	1.0	1.6
TY-2C	Ti 1.25	$Ar + 2\%O_2$	20	1.1	2.3
TY-3A	Ti 2.50	Ar	20	0.9	2.7
TY-3B	Ti 2.50	$Ar + 5\%H_2$	20	0.9	1.7
ZY-1A	Zr 0.15	Ar	20	1.0	1.5
ZY-1B	Zr 0.15	$Ar + 5\%H_2$	20	1.0	1.6
ZY-1C	Zr 0.15	$Ar + 2\%O_2$	20	0.9	1.6
ZY-2A	Zr 0.75	Ar	20	1.0	2.0
ZY-2B	Zr 0.75	$Ar + 5\%H_2$	20	1.0	2.0
ZY-2C	Zr 0.75	$Ar + 2\%O_2$	20	1.0	2.4
ZY-3A	Zr 1.50	Ar	20	1.3	1.9
ZY-3B	Zr 1.50	$Ar + 5\%H_2$	20	1.0	1.9
CY-1B	Cr 0.25	$Ar + 5\%H_2$	20	0.9	1.5
CY-1C	Cr 0.25	$Ar + 2\%O_2$	20	0.9	2.1

beams, leading to a quenched molten zone in a number of growth runs.

2.2. Fiber Characterization

Powder X-ray diffraction (XRD) measurements were carried out in the 2θ range of 15–100° on a Rigaku RU-300 diffractometer operated at 50 kV, 200 mA. The lattice constants of the grown fibers were determined using Si as an internal standard in order to assess the solubilities of the dopants into YAG both as a function of concentration and valence state. The determination of the lattice constants were performed using the peaks in the 2θ range of 85–110° after making corrections for absorption, and horizontal and vertical divergences as well as errors caused by misalignments of apparatus and sample displacement [22,23].

Quantitative analyses for composition were carried out by electron probe microanalysis (EPMA) with a wavelength-dispersive spectrometer (WDS). Typical detection limits of the technique are 0.01–0.05at.%, depending on the dopant element. Usually, the sensitivity to Ti is better than the others since the count rate of the characteristic X-ray for Ti is much higher. Y and Al contents were also measured simultaneously. Specimens for EPMA were polished along the growth direction with 12 μm, 1 μm and 0.056 μm alumina abrasives, then the surface was coated with a 250 Å thick carbon film to prevent charge-up induced by the electron beam during analysis. The analysis was performed with a beam diameter of 1 μm on a JEOL Superprobe 733, operating at a beam current of 10–20 nA and a voltage of 15 kV using YAG, TiO_2 and ZrO_2 as standard materials.

3. Results and Discussion

3.1. YAG Fiber Growth by the LHFZ Technique

During the LHFZ growth from polycrystalline feed rods with square cross section, a few unfavorable phenomena typically occurred, including bubble generation in the melt zone and irregular melting of the feed rod. Especially under Ar and $Ar + 2\%O_2$ atmospheres, bubble formation occurred during growth of Ti- and Zr-doped fiber even when dense feed rods ($> 95\%$) were employed. In contrast, severe bubbling from the melt was seen in $Ar + 5\%H_2$ atmosphere for the growth of Cr-doped YAG fibers. The bubbles disturbed or terminated growth at times by inducing abrupt changes in the zone shape and/or breakdown of the melt zone. Formation of bubbles appears to depend on the growth atmosphere. As for the Ti- and Zr-doped fibers, the bubbles decreased drastically under a reducing atmosphere of $Ar + 5\%H_2$, while a great number of bubbles were seen during growth in Ar or $Ar + 2\%O_2$ gas. For the Cr-doped fibers, however, the opposite occurred. As a result, a relatively high density of microvoids (typically less than 1 μm in size as observed by the optical microscope) were observed in some fibers even though the fibers were pulled downward so as to avoid the accumulation of bubbles at the growth interface. Longer melt zones and multiple zone-passes decreased the density of microvoids to some degree. The microvoids tended to accumulate with the growth length, particularly at the periphery of the fiber, as illustrated in Fig. 2. The other problem of irregular

Fig. 2. Microvoids (black points) observed at the growth length of 18 mm in a 22 mm long undoped YAG fiber grown in $Ar + 2\%O_2$. A significant accumulation of microvoids is seen at the periphery of the fiber. Cracks exist in the upper part of the photograph.

melting of square cross-sectional feed rods led to fluctuations in melt volume, and corresponding perturbations in dopant segregation [24]. In addition, an instability of the melt zone shape occurred in all growth runs from heavily Ti-doped YAG feed rods (e.g. 2.5at.%).

The color of grown YAG fibers varied with dopant. In general, grown YAG fibers were brown for Ti-doped, red for Zr-doped, and light green for Cr-doped YAG fibers, respectively. The intensity of the color increased with dopant concentration. In addition, the color of the Ti- and Zr-doped fibers grown in $Ar + 5\%H_2$ were more intense than that of fibers grown in Ar. However, Cr-doped YAG fibers grown in $Ar + 5\%H_2$ were almost colorless, while those grown in $Ar + 2\%O_2$ were light green. In spite of low concentrations (less than 0.15at.%), Zr-doped fibers display relatively intense color, as compared with Ti-doped fibers with the same dopant level. All the fibers, grown in $Ar + 5\%H_2$, typically exhibited a frosted surface as compared with those grown in Ar or $Ar + 2\%O_2$.

3.2. *Precipitation*

Precipitation of second phases is of major concern in the growth of heavily doped fibers. In general, a precipitate is formed when the dopant concentration of the melt at the growth interface reaches a solubility limit (eutectic concentration). For growth at high crystallization rates in a steep temperature gradient like in this study, the precipitate formation is usually influenced by growth kinetics as well as thermal history after crystallization. For instance, the morphology of the precipitate is expected to significantly depend not only on the growth rate but also the growth interface shape. Due to limited growth experiments on the growth rate dependency in this study, a critical dopant concentration C_P, instead of an equilibrium solubility limit, was defined as the dopant concentration of a YAG matrix in the region where precipitation began in grown fibers. The values are summarized in Table 3, as well as the nature of the precipitates identified by EPMA and/or XRD.

In Ti-doped YAG, the critical dopant concentration was found to exceed 2.5at.% in $Ar + 5\%H_2$ with the concentration not yet determined. Precipitates of $Y_2Ti_2O_7$ were observed about 0.75at.% Ti in the Ar-grown fiber (TY-3A) by means of EPMA. Although

Table 3. Critical dopant concentration and precipitates observed in grown fibers

Dopant	Atmosphere	Critical concentration C_p(at.%)	Precipitates	Fiber No.
Ti	$Ar + 5\%H_2$	> 2.50	not observed	TY-3B
Ti	Ar	0.75	$Y_2Ti_2O_7$	TY-3A
Ti	$Ar + 2\%O_2$	> 0.35	not observed	TY-2C
Zr	$Ar + 5\%H_2$	0.23	YZr_2O_x	ZY-2B, ZY-3B
Zr	Ar	0.20	YZr_2O_x	ZY-2A, ZY-3A
Zr	$Ar + 2\%O_2$	0.12	$YZrAl_5O_x$	ZY-2C

precipitates were not found up to 0.35at.% for the case of $Ar + 2\%O_2$, the precipitation is thought to strongly depend on growth atmosphere for Ti in YAG. The precipitates found in the Ar-grown fiber (TY-3A), as shown in Fig. 3, were of a columnar shape, elongated parallel to the growth direction with a 1–5 μm wide and 10–30 μm long size.

In contrast, Zr showed only a weak dependence in the critical dopant concentration ranging 0.1–0.2at.%, as compared with Ti. The difference in the concentra-

Fig. 3. SEM micrograph (back-scattered electron image) of $Y_2Ti_2O_7$ precipitates (white phase) in the Ti-doped YAG fiber (TY-3A) grown from a 2.5at.% Ti-doped feed rod in pure Ar atmosphere.

tion seems to originate from the multiplicity of valence states of the dopants. Ti is normally observed in two valence states i.e., Ti^{3+} and Ti^{4+}, with Ti^{3+} expected to be more highly incorporated into the YAG lattice in light of its isovalent character vis-a-vis Al^{3+}. Unlike Ti, Zr is typically only Zr^{4+} and thus requires defect formation to satisfy electroneutrality.

Previously, Zr-doped crystals have been grown from melts containing up to 2wt.% ZrO_2 (corresponding to ≈ 0.5at.%), and the deterioration of the crystal quality was found when the ZrO_2 concentration of the melt was beyond 2wt.% [13]. Although the precipitation was not explicitly described in the previous work, the result is nearly consistent with the critical concentration, 0.1–0.2at.%, found in this study, assuming the segregation coefficient of the order of 0.1.

In the case of Zr-doped fibers grown in Ar and $Ar + 5\%H_2$, there were two major second phases found other than the YAG phase. The one phase had the composition of Y:Zr = 1:2 with typical diameter of 1–5 μm, as shown in Fig. 4. The other was not identified due to difficulty in analysis. In the $Ar + 2\%O_2$ case, instead of those phases, precipitates with the composition of Y:Zr:Al = 1:1:5 were observed at the critical concentration, 0.12at.%, which was slightly lower than that of the Ar and $Ar + 5\%H_2$ case (Fig. 5). The precipitates in the Ar- and Ar/H_2-grown fibers seem to be formed along the growth interface, which is convex to the melt from the observation of the quenched fiber, with a regular interval of 100–200 μm for nominally 1.5at.% Zr-doping, or 15–25 μm for 0.75at.% Zr-doping parallel to the growth direction. The periodic formation of the precipitates can be typically caused by the oscillation

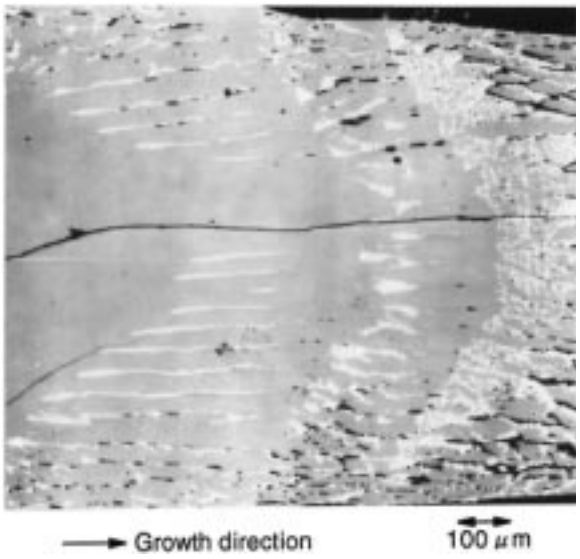

Fig. 4. YZr_2O_x precipitates (white phase on the back-scattered electron image) in the Zr-doped YAG fibers.
(a) Fiber (ZY-3A) grown from 1.5at.% Zr-doped feed rod in Ar.

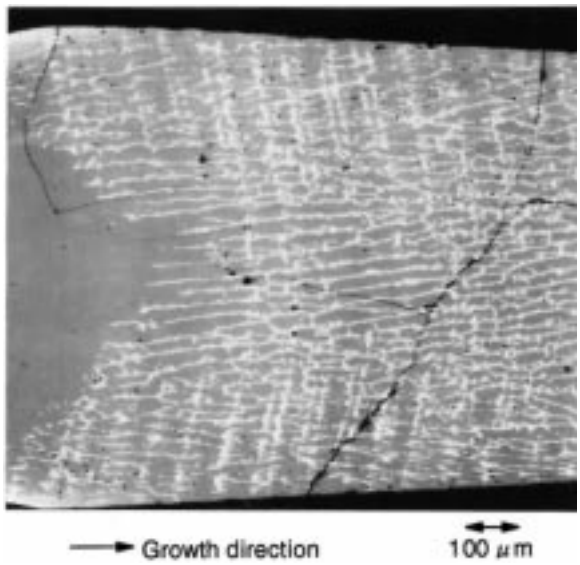

(b) Fiber (ZY-3B) grown from 1.5at.% Zr-doped feed rod in $Ar + 5\%H_2$.

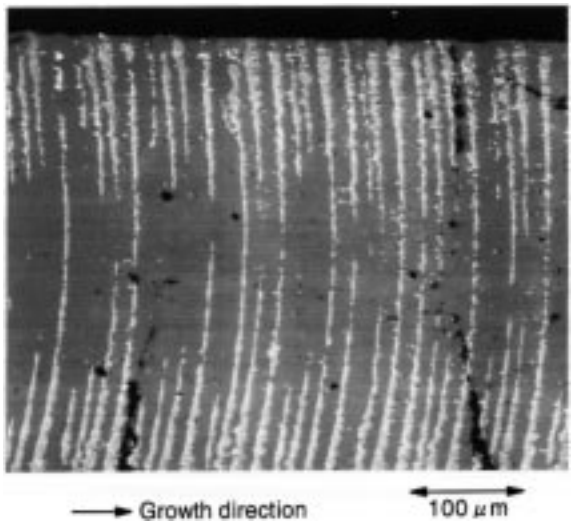

(c) Fiber (ZY-2B) grown from 0.75at.% Zr-doped feed rod in $Ar + 5\%H_2$.

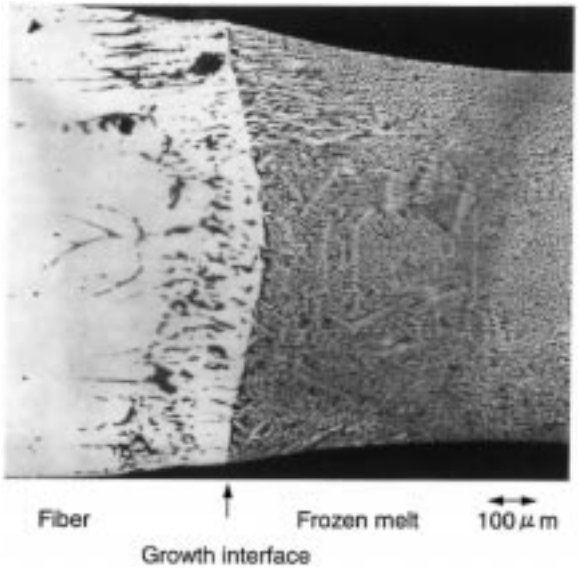

Fig. 5. SEM micrograph of precipitates (gray phase in the fiber) with the composition of Y:Zr:Al = 1:1:5 in the Zr-doped fiber (ZY-2C) grown in Ar + 2%O_2 (back-scattered electron image).

of the interface dopant concentration around the solubility limit. Such concentration oscillation is often induced by the fluctuation in the growth rate originated from the perturbations in melt volume and temperature. Further, at the initial stage of the precipitation in Fig. 4(a) and 4(b), columnar precipitates, elongated to the growth direction with an interprecipitate distance of 30–50 μm, primarily appeared, suggesting cellular growth. In contrast, the Ar/O_2-grown case displayed precipitates with an irregular shape.

No precipitates of Cr were observed in fibers grown either in reducing (CY-1B) or oxidizing (CY-1A) atmospheres. Therefore, the critical concentration could not be determined. Moreover, the fiber and quenched melt exhibited no Cr within the detection limit for the Ar/H_2-atmosphere case. An extremely low Cr concentration was found in both the fiber and the melt near the growth interface in the Ar/O_2 case. These results strongly indicate an evaporative loss of Cr during growth. The evaporative loss of Cr was observed also in Cr-doped Al_2O_3 grown by the LHFZ method in Ar/H_2 atmosphere [11]. Hence, Cr evaporation seems to be crucial in the growth of Cr-doped YAG fibers. This evaporative loss will be discussed in more detail later.

The dopant solubility is typically a function of temperature as well as atmosphere. The dopant incorporation in this study was likely established at temperatures just below the melting point (1970°C) since very steep temperature gradients (typically 10^3–10^4°C/cm) tend to freeze in the high temperature state in grown fibers. Therefore, precipitates may come out when the fibers are annealed at a lower temperature and/or in different atmospheres after growth. After heat treatment in an oxidizing atmosphere (air), in general, Ti-doped fibers became discolored and small precipitates of Ti oxides appeared in the matrix. Although the temperature dependence of the solubility limit was not examined, even crystals doped with 0.05–0.08at.% Ti exhibited a great number of Ti-rich precipitates, as shown in Fig. 6, with dimensions less than 1 μm (presumably $Y_2Ti_2O_7$) after annealing in the 1100–1400°C range for 5–24 h in air. A decrease in Ti concentration in the matrix was observed as a result of the precipitation (e.g. reduction from 0.05–0.08at.% to 0–0.03at.% in the matrix near the precipitates in Fig. 6).

On the other hand, annealing at 1550°C for 24 h in a reducing atmosphere (a flowing gas of 0.1% CO_2/CO, $PO_2 = 8 \times 10^{-14}$ atm) gave rise to a certain amount of precipitates present only on the surface of

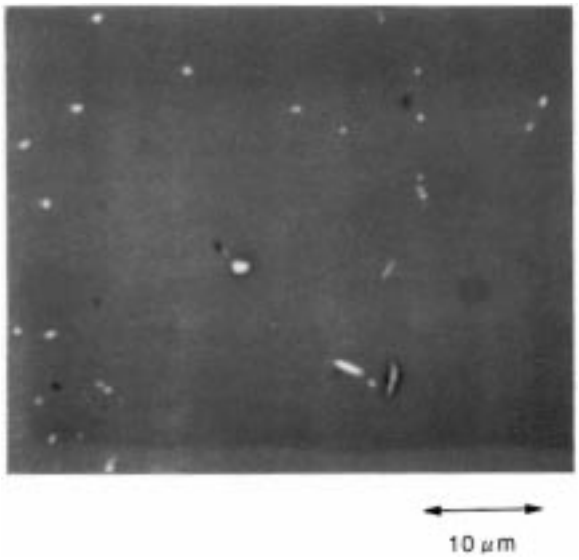

Fig. 6. Precipitates of Ti-rich oxides (presumably $Y_2Ti_2O_7$) after annealing in the 1100–1400°C range under an oxidizing atmosphere (air) in a Ti-doped YAG crystal. The crystal, which had been grown in Ar + 2%H_2 atmosphere, has 0.050–0.08at.% Ti in the matrix and showed no precipitates before the annealing.

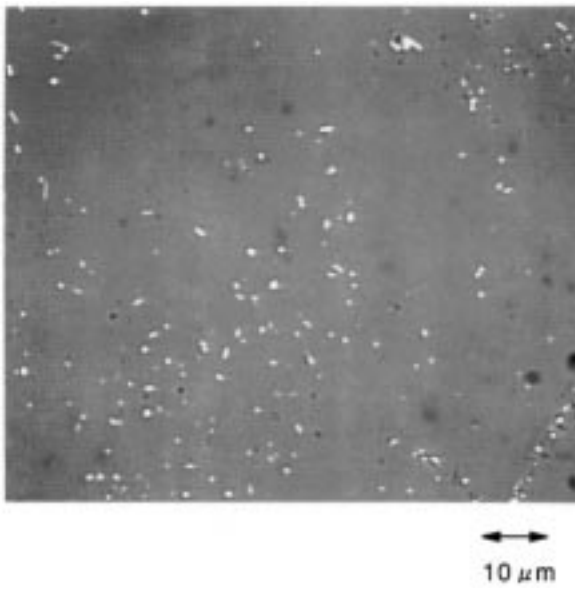

Fig. 7. Surface precipitates (white phase) formed in a 0.25at.% Ti-doped YAG fiber after annealing at 1550°C for 24 h in a flowing 0.1% CO_2/CO mixed gas ($PO_2 = 8 \times 10^{14}$ tm).

0.25at.% Ti-doped fibers (see Fig. 7). Mo precipitates were previously reported in YAG crystals which have been grown in a Mo crucible and then annealed in H_2 [11]. However, the precipitates observed in this study were of a Ti-rich phase and small, typically less than 1 μm in size, and appear to be related to an atmosphere-dependent segregation phenomenon. As for Zr-doped fibers containing 0.06at.% Zr, however, no precipitates were formed by annealing at 1100–1400°C for $\approx$12 h in an oxidizing or reducing atmosphere.

3.3. Compositional and Structural Variation with Doping

YAG has the garnet structure containing three different cation sites in the lattice [25]. Y^{3+} ions reside at 8-fold coordinated dodecahedral sites (c-sites) while Al^{3+} ions are located on both 6-fold coordinated octahedral sites (a-sites) and 4-fold coordinated tetrahedral sites (d-sites). The ionic radii of the cations are 1.015 Å, 0.39 Å and 0.53 Å for the c-site Y^{3+}, the d-site Al^{3+} and the a-site Al^{3+}, respectively. In light of their typical coordination sites and their ionic radii, Ti (0.61–0.86 Å) and Cr cations (0.55–0.73 Å) are predicted to replace Al at the a-sites. In contrast, the relatively larger Zr cations (0.84 Å) are believed to be primarily incorporated on the c-site [13].

The compositional variations of Y and Al as a function of dopant concentration are illustrated in Fig. 8. In the Ti-doped YAG fibers, the Al content is decreasing at a ratio of one to one with increasing Ti concentration, while the Y content remains nearly

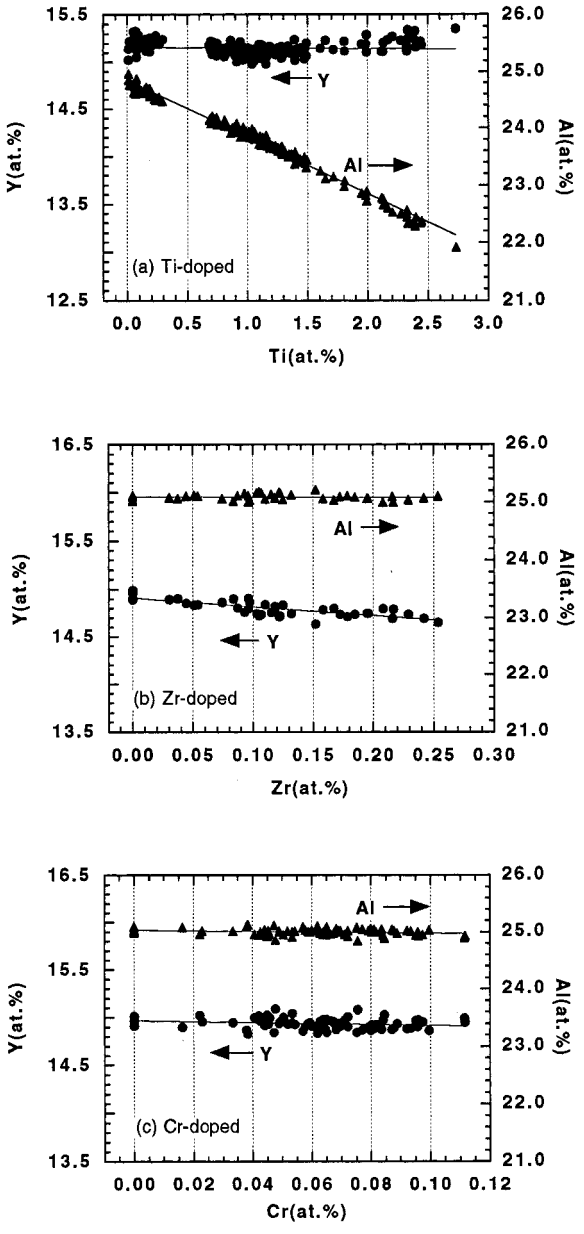

Fig. 8. Compositional change in Y and Al as a function of (a) Ti, (b) Zr or (c) Cr concentration in grown YAG fibers.

constant. This confirms that Ti substitutes for Al as expected. In the Zr-doped YAG case, the Y content is found to decrease with increasing dopant concentration, maintaining a constant Al content. However, compositional change was not detected for the Cr-doped YAG because of the low dopant concentrations, ranging from nearly zero to 0.1at.%.

In the powder X-ray diffraction measurements, a shift of the diffraction peaks was found with doping for the Ti-doped YAG fibers, indicating a variation of the lattice constant (see Fig. 9). According to more precise measurements for selected Ti-doped YAG fibers with no precipitates, the lattice constant increases linearly with increasing Ti percentage $x(\%)$ for $Y_3(Al_{1-x}Ti_x)_5O_{12}$, as shown in Fig. 10. The relation is expressed by the following equation.

$$a(\text{Å}) = 12.008 + 0.0053x(\%) \qquad (1)$$

The variation exhibits fairly good agreement with that calculated by the empirical equation assuming that Ti^{3+} (0.67 Å) ions reside on the a-sites in the YAG lattice rather than Ti^{4+} (0.605 Å) or Ti^{2+} (0.86 Å) [26], confirming that our assumptions were reasonable. Moreover, these are consistent with the fact that a large number of $Y_2Ti_2O_7$ precipitates were formed when annealing in air, in which more Ti^{4+} cations were generated. In Zr-doped YAG fibers, a decrease in the lattice constant is expected if the smaller Zr^{4+} replaces the Y^{3+}. However, no significant change in lattice constant, which was determined to be 12.011Å, could be observed within experimental error.

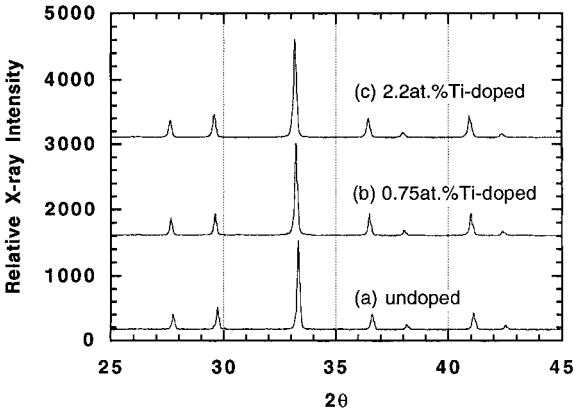

Fig. 9. Powder X-ray diffraction patterns for: (a) undoped YAG fiber, (b) 0.75at.% Ti-doped YAG fiber, and (c) 2.2at.% Ti-doped YAG fiber.

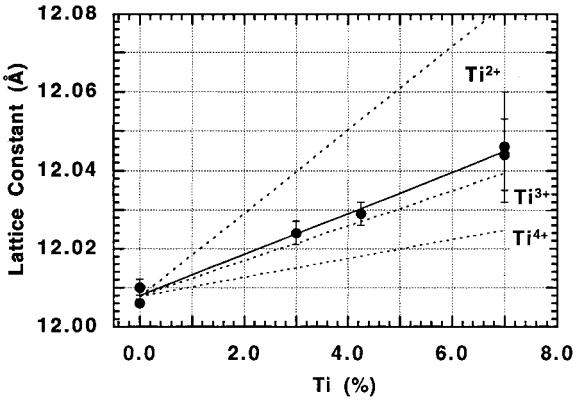

Fig. 10. Variation of lattice constant as a function of Ti percentage x (%) for $Y_3(Al_{1-x}Ti_x)_5O_{12}$.

3.4. Theory of Dopant Distributions in Zone Melting

When the molten zone is passed along the feed rod only once, the dopant variation along the growth direction is described as a function of growth length, x, by Pfann's equation [10] where constant parameters, zone length and cross section, dopant concentration in feed rod, effective segregation coefficient, radius of fiber and radius of feed rod, are assumed as well as no evaporative loss of dopant. In real growth, however, the evaporation of the dopant is more likely as well as radius change between feed rod and fiber. In this case, a dopant consumption due to evaporation from the melt, and a ratio of crystallization to melting in a given time should be taken into account for modification of Pfann's equation. The evaporation of dopant during zone melting was studied by Boomgaard for an ideal case in which growth was carried out under a constant vapor pressure of dopant in equilibrium with the melt [27]. Ziegler then applied the analysis to a special case of growth in a vacuum [28]. In this study, the analysis model was based on the latter case since our growth conditions, an open or cold-wall system, was more similar to that rather than the constant vapor-pressure case. According to the theory, the evaporative loss from the melt is proportional to both the ratio of the surface area to the volume of the melt zone and the dopant concentration in the melt with a parameter g, which characterizes the evaporation rate. Taking account of the change in the pulling rate between

fiber and feed rod, the differential equation for dopant concentration follows.

$$dC_m = (\pi R^2 C_s/V_m)dx_0 - (\pi r^2 k_{eff} C_m/V_m)dx - g(S_m/V_m)C_m dt \quad (2)$$

where

C_m(at.%): Dopant concentration in melt,
C_s(at.%) : Dopant concentration in feed rod,
k_{eff} : Effective segregation coefficient,
g(mm/min) : Evaporation constant of dopant,
V_m(mm^3) : Melt volume, S_m(mm^2) : Surface area of melt
x, x_0(mm) : Position of fiber and feed rod in the growth direction, in steady state, $R^2 dx_0 = r^2 dx$ from requirement of mass conservation,
R(mm) : Radius of feed rod, r(mm): radius of grown fiber,
t(min) : time, v(mm/min) : Growth rate, $x = vt$

From the relation $C_F = k_{eff}\ C_m$, the dopant concentration in the fiber, C_F becomes

$$\begin{aligned} C_F(x) &= (\alpha/\beta)k_{eff}C_S[1 - \exp(-\beta x/v)] \\ &\quad + k_{eff}C_i \exp(-\beta x/v) \\ &= (\alpha/\beta)k_{eff}C_S \\ &\quad + k_{eff}[C_i - (\alpha/\beta)C_S] \exp(-\beta x/v) \end{aligned} \quad (3)$$

with

$$\begin{aligned} C_i &= C_m(x = 0, t = t_i) \\ &= C_s \exp[-(g/\gamma)t_i] \end{aligned} \quad (4)$$

t_i : time interval between melting of feed rod and initiation of pulling

$$\begin{aligned} \alpha &= \pi r^2 v/V_m \\ &= 3r^2 v/[h(R^2 + rR + r^2)] \end{aligned} \quad (5)$$

$$\beta = \alpha k_{eff} + g/\gamma \quad (6)$$

$$\begin{aligned} \gamma &= V_m/S_m \\ &= h(R^2 + rR + r^2)/[3(R + r) \\ &\quad \times \{(R - r)^2 + h^2\}^{1/2}] \end{aligned} \quad (7)$$

In the Eqs. (5) and (7), the melt volume, V_m, may be calculated using a zone height h in a manner where the molten zone shape is a simple truncated cone instead of the more complex shape of the actual molten zone. For no evaporative loss of the dopant, $g = 0$, Eq. (3) can be reduced to the following equation, which will be identical to the conventional equation by Pfann, where $R = r$.

$$\begin{aligned} C_F(x) &= C_S[1 + (k_{eff} - 1) \exp(-\alpha k_{eff} x/v)] \\ &= C_S[1 + (k_{eff} - 1) \exp(-k_{eff} x/h)] \end{aligned} \quad (8)$$

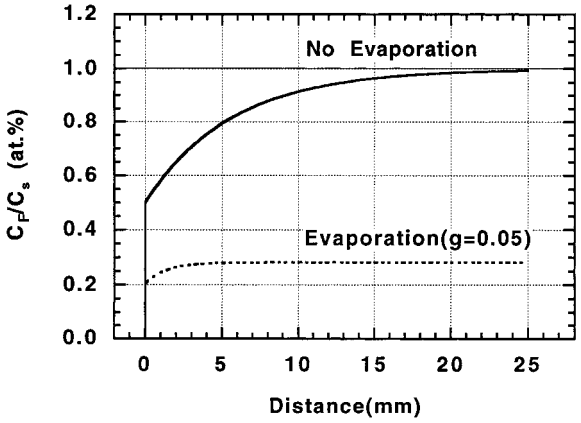

Fig. 11. Dopant distribution with and without evaporation loss calculated using the following parameters: $R = 0.6$ mm, $r = 0.5$ mm, $h = 2$ mm ($\alpha = 0.14$ mm^{-1}, $\gamma = 0.28$ mm), $v = 20$ mm/$h = 0.333$ mm/min, $k_{eff} = 0.5$, $g = 0.05$, $t_i = 5$ min.

Calculated distributions of dopant are illustrated in Fig. 11 for the cases both with and without evaporative loss based on Eq. (3). The dopant concentration increases with growth distance, and then reaches a steady-state value in a certain length. In the case of no evaporation, the steady-state concentration should be equal to the dopant concentration of the feed rod, C_S, while for the evaporative case a steady-state concentration less than C_S is expected in a shorter length. Effective segregation coefficient and evaporation constant can be determined by fitting the data to Eq. (3).

3.5. Dopant Distributions and Estimation of Effective Segregation Coefficients

All the dopant concentrations were measured in the YAG matrix excluding precipitates. The analysis was performed on the centerline of a longitudinal cross-section of the fiber along the growth direction. Axial

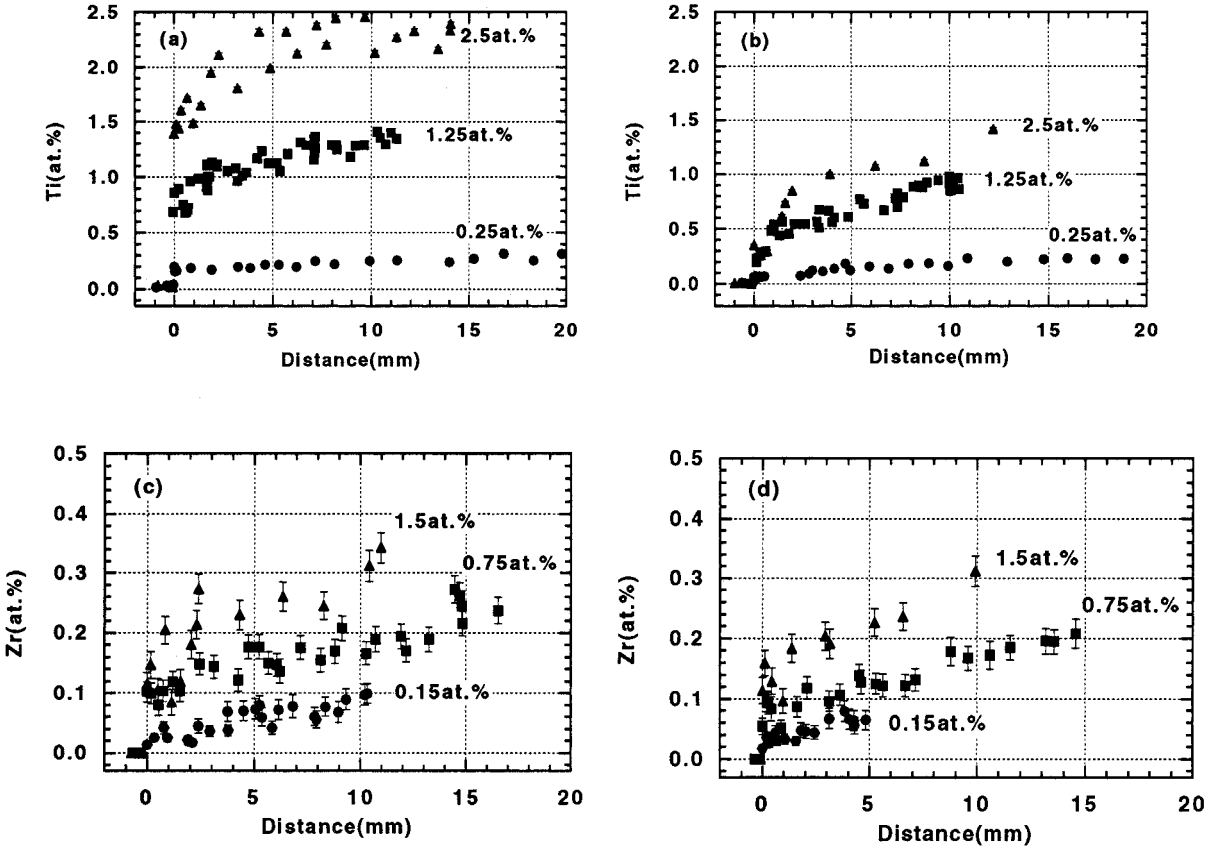

Fig. 12. Dopant distributions of Ti- and Zr-doped YAG fibers in Ar and Ar + 5%H_2: (a) Ti-doped YAG fibers grown in Ar + 5%H_2, (b) Ti-doped YAG fibers grown in Ar, (c) Zr-doped YAG fibers grown in Ar + 5%H_2, (d) Zr-doped YAG fibers grown in Ar.

dopant distributions of the Ti- and Zr-doped fibers are shown in Fig. 12. The zero-point of the distance, that is the seeding point, in Fig. 12 was determined by the observation of a discontinuity in the dopant concentration. During analysis of the axial dopant concentration profile, a microscopic fluctuation of the dopant concentrations was observed as well. This issue is also important for understanding of dopant behavior, but beyond the scope of this study. This will be discussed in more detail elsewhere [29].

In the Ti-doped fibers grown in Ar + 5%H_2, the Ti concentration increases rapidly up to the nominal doping level in the feed rods. Typically, the concentration reaches the nominal doping level of the feed rod at approximately 10 mm. After that, the dopant concentration is kept constant by zone-leveling in which the input and output of dopant to melt is equal. In contrast, in the Ar case, only the fiber grown from the 0.25at.% Ti-doped feed rod shows the same kind of variation. In the cases of 1.25at.% and 2.5at.% Ti-doped feed rods, there is a slight bending of curves around 0.75at.%, where precipitation occurs. The strong variation with atmosphere is shown in Fig. 13.

As for Zr-doped fibers, the concentration increases more slowly than that of Ti-doped fibers with distance in all atmospheres (Fig. 12), exhibiting little change with growth atmosphere (Fig. 14). Unlike Ti, the Zr concentration exhibits no steady-state at the maximum growth length in all the fibers, suggesting a low segregation coefficient with either zero or small evaporative constant. Therefore, the segregation coefficient and evaporation constant should be determined by Eq. (3) taking into account evaporation of dopant. Precipitates were found about $\approx$0.2at.% in the fibers grown from the 1.5at.% and 0.75at.% Zr-doped feed rods in Ar and Ar + 5%H_2 atmospheres.

Cr-doped fibers display an extreme change with atmosphere, as illustrated in Fig. 15. No Cr was detected within detection limits in the fiber grown in

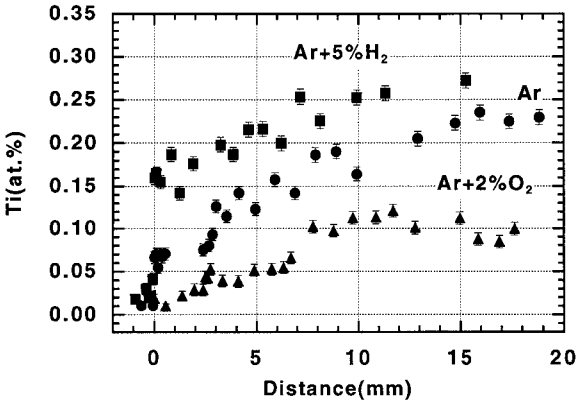

Fig. 13. Dopant distributions of Ti-doped YAG fibers grown from 0.25at.% Ti-doped feed rods in the different atmospheres.

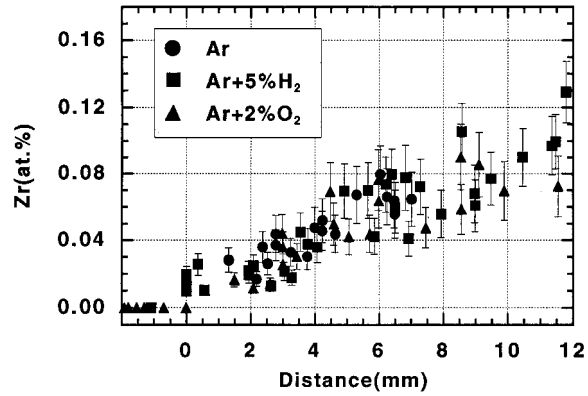

Fig. 14. Dopant distributions of Zr-doped YAG fibers grown from 0.15at.% Zr-doped feed rods in the different atmospheres.

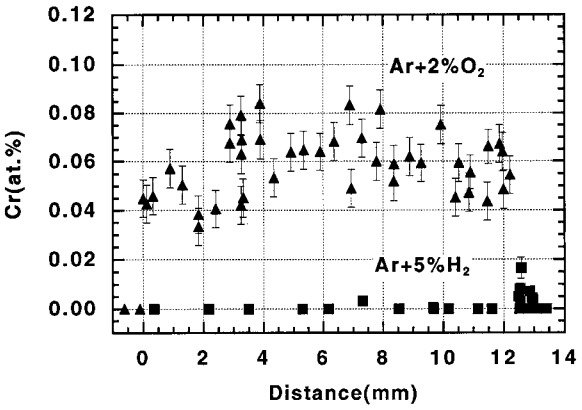

Fig. 15. Dopant distributions of Cr-doped YAG fibers grown from 0.25at.% Cr-doped feed rods in the different atmospheres.

$Ar + 5\%H_2$. On the other hand, the Ar/O_2-grown fiber showed an almost uniform concentration of 0.05–0.08at.% throughout the fiber, indicating a characteristic of the evaporation case.

Effective segregation coefficients of the dopants were calculated by a curve fit, using effective segregation coefficient k_{eff} and vaporization constant g as fitting variables, to the experimental dopant distributions in the precipitate-free fibers, based on the segregation mode (see Eq. (3)) of the zone melting. Although scatter in the data associated with the microscopic fluctuation in the dopant concentration was seen to some degree, segregation coefficients could be estimated with reasonable precision, as listed in Table 4. Generally, segregation coefficients also depend strongly on both growth rate and growth direction [10], which, in this study, have been fixed at 20 mm/h and the [111] direction.

All the Ti-doped fibers followed the segregation theory for the case of no evaporation, showing a significant growth atmosphere dependence of effective segregation coefficients. Like the atmosphere dependence of the critical dopant concentration for precipitation, Ti^{3+} is expected to be more preferable for incorporation into the Al^{3+} site of the YAG lattice than Ti^{4+}, which forms in oxidizing atmospheres. Previously, effective segregation coefficients of Ti in Bridgman-grown crystals were estimated to be roughly 0.1 and 0.3 in He and H_2 atmospheres, respectively [12]. The values obtained in this study are greater than those, possibly due to the higher growth rate as compared with that of 1.5–10 mm/h in the Bridgman method [10]. As for Zr, the segregation coefficients were determined to be approximately 0.1 in all the atmospheres. Zr has a single valence state of Zr^{4+} [21], which is obviously unfavourable for substitution of the Y^{3+} cation. Like the Ti-doped fibers, Zr-doped fibers showed no evaporative loss of Zr.

Concerning Cr-doped fibers, no Cr was detected in the fiber grown in $Ar + 5\%H_2$. Low concentrations of Cr could be detected in fibers grown in $Ar + 2\%O_2$, but the concentration was saturated at a much lower level than that of the feed rod. Furthermore, no precipitates containing Cr were observed, and the Cr concentrations in frozen melts were considerably lower than those of the feed rods, less than 0.02at.% and 0.05–0.1at.% for the cases of $Ar + 5\%H_2$ and $Ar + 2\%O_2$, respectively. These results clearly indicate that significant evaporative loss of Cr occurred

Table 4. Summary of effective segregation coefficients k_{eff}, evaporation constant g, and parameters used for estimation

Fiber no.	Dopant	C_s (at.%)	Atmosphere	α (min^{-1})	γ (mm)	k_{eff}	g (mm/min)
TY-1B	Ti	0.25	$Ar+5\%H_2$	0.145	0.276	0.63	0.00
TY-2B	Ti	1.25	$Ar+5\%H_2$	0.147	0.294	0.63	0.00
TY-3B	Ti	2.50	$Ar+5\%H_2$	0.140	0.263	0.60	0.00
TY-1A	Ti	0.25	Ar	0.123	0.276	0.26	0.00
TY-2A	Ti	1.25	Ar	0.114	0.283	0.28	0.00
TY-1C	Ti	0.25	$Ar+2\%O_2$	0.107	0.277	0.11	0.00
ZY-1B	Zr	0.15	$Ar+5\%H_2$	0.169	0.275	0.13	0.00
ZY-1A	Zr	0.15	Ar	0.181	0.275	0.11	0.00
ZY-1C	Zr	0.15	$Ar+2\%O_2$	0.183	0.238	0.10	0.00
CY-1C	Cr	0.25	$Ar+2\%O_2$	0.118	0.264	0.9	0.09

Assuming $\alpha = 3r^2v/[h\,(R^2+rR+r^2)]$, $\gamma = h\,(R^2+rR+r^2)/[3(R+r)\,\{(R-r)^2+h^2\}^{1/2}]$, and using $t_1 = 5$ min (exptl. value).

from the melt. In fact, Cr or CrO is known to be volatile at high temperatures in a reducing atmosphere. Provided that evaporative loss of the dopant is taken into account, the effective segregation coefficients, k_{eff} and evaporation constant, g are then estimated by the modified zone melting model. From the fit between the calculated curve and analysis data, two possible combinations of effective segregation coefficient and evaporation constant were obtained due to the relatively large error associated with the analysis. These values are $k_{eff} = 0.9 \pm 0.3$ with $g = 0.09 \pm 0.03$ mm/min, and $k_{eff} = 0.3 \pm 0.1$ with $g = 0.03 \pm 0.01$ mm/min, respectively (see Fig. 16). However, the former case was finally taken since the segregation coefficient was found to be 0.09–1.0 by the analysis of the Ti concentration ratio between the fiber and melt at the growth interface in a quenched fiber. As for the segregation coefficient of Cr in YAG, there have been a few controversial results reported, for example 0.1 by Kvapil et al. [30] and approximately 2 by Kitamura et al. [31], for Czochralski crystals grown typically in a reducing atmosphere with a lower growth rate. The value estimated in this study also exhibits a disagreement with both results probably due to both the atmosphere-dependent evaporation phenomena and the difference in growth rate. There is no study on the evaporation constant of Ti in YAG growth, but that of Ti in Al_2O_3 was reported to be $g = 0.11$ mm/min [32]. In summary, Cr has a large effective segregation coefficient combined with high evaporative losses.

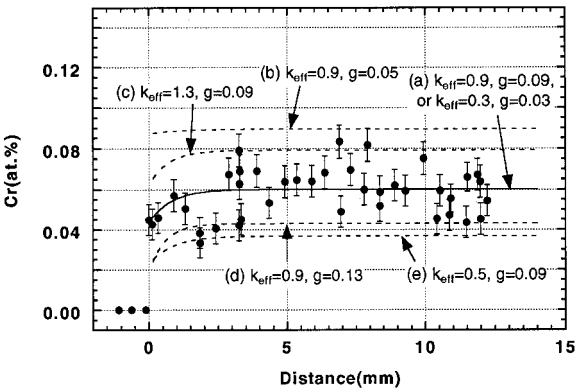

Fig. 16. Experimental and calculated dopant distributions of Cr-doped YAG fiber grown from 0.25at.% Cr-doped YAG fiber in $Ar+2\%O_2$. Calculated lines are made with the parameters: (a) $k_{eff} = 0.9$, $g = 0.09$, or $k_{eff} = 0.3$, $g = 0.03$, (b) $k_{eff} = 0.9$, $g = 0.05$, (c) $k_{eff} = 1.3$, $g = 0.09$, (d) $k_{eff} = 0.9$, $g = 0.13$, (e) $k_{eff} = 0.5$, $g = 0.09$.

4. Conclusion

The incorporation of Ti, Zr and Cr into YAG fibers has been systematically investigated using approximately 1 mm-diameter fibers grown from polycrystalline feed rods with nominal dopant concentrations of 0.15–2.5at.%, in the three atmospheres of $Ar+2\%O_2$ and Ar and $Ar+5\%H_2$. Electron probe microanalysis (EPMA) revealed that the axial distribution and the precipitation of the dopants were strongly influenced by the growth atmosphere in Ti and Cr-doped fibers, but not in Zr-doped fibers. These atmosphere dependencies are induced not only by the variation of the effective segregation coefficients and solubility with growth atmosphere, but also by evaporative loss of the dopants from the melt. In some cases, especially in

the Cr-doped fibers, the effect of the evaporative loss from the melt is very prominent, such that the resultant changes of the composition in the melt provide unusual distributions of dopants.

The effective segregation coefficients in the different atmospheres were estimated from the axial distributions of the dopants using the dopant segregation equations for the cases with and without evaporative loss. The segregation coefficient of Ti varied strongly with the growth atmosphere, while that of Zr is nearly constant at approximately 0.1 in all atmospheres. Cr exhibited a value close to unity but suffered from high volatility. Consequently, the concentration of Cr in YAG remained fairly low. The growth atmosphere dependence of the effective segregation coefficients and precipitation in the Ti-doped fibers is to be expected by the change of the valence state of Ti with atmosphere.

Acknowledgment

This work was supported, in part, by Sumitomo Electric Industries, Ltd., an AT&T Bell Laboratory Fellowship (J.K.W.C.) and the Sumitomo Electric Industries faculty chair (H.L.T.). We would like to thank Dr. J.S. Haggerty and Dr. J. Sigalovsky for useful discussions on crystal growth and the use of the laser growth systems. We also acknowledge the assistance of Drs. Michael J. Jercinovic and Nilanjan Chattenzee with EPMA and the use of the Center of Materials Science and Engineering (MRSEC) central facilities.

References

1. S.R. Rotman and H.L. Tuller, *J. Appl. Phys.*, **62**, 1305 (1987).
2. S.R. Rotman, M. Roth, H.L. Tuller, and C. Warde, *J. Appl. Phys.*, **66**, 1366 (1989).
3. S.R. Rotman, C. Warde, H.L. Tuller, and J.S. Haggerty, *J. Appl. Phys.*, **66**, 3207 (1989).
4. J. Kvapil, Jos. Kvapil, J. Kubelka, and B. Perner, *Czech. J. Phys.*, **B32**, 817 (1982).
5. J. Kvapil, Jos. Kvapil, and B. Perner, *Kristall und Technik*, **10**, 161 (1975).
6. J. Kvapil, B. Perner, Jos. Kvapil, and K. Blazek, *Kritall und Technik*, **15**, 1163 (1980).
7. D. Peizhen, Q. Jingwen, H. Bing, Z. Yongzong, and Z. Meizhen, *J. Crystal Growth*, **92**, 276 (1988).
8. D. Petrova, O. Pavloff, and P. Marinov, *J. Crystal Growth*, **99**, 841 (1990).
9. A.M. Balbashov and S.K. Egorov, *J. Crystal Growth*, **52**, 498 (1981).
10. W.G. Pfann, in *Zone Melting* (John Wiley & Sons, New York. 1958).
11. J.S. Haggerty, K.C. Wills, and J.E. Sheehan, *Ceram. Eng. Sci. Proc.*, **12**, 1785 (1991).
12. I.I. Karpov, *Sov. Phys. Crystallogr.*, **23**, 710 (1978).
13. P. Peshev, V. Petrov, and N. Manuilov, *Mat. Res. Bull.*, **23**, 1193 (1988).
14. H.R. Asatryan, A.S. Kuzanyan, A.G. Petrosyan, A.K. Petrosyan, and E.G. Sharoyan, *Phys. Stat. Sol.*, (b)**135**, 343 (1986).
15. C.A. Burrus and J. Stone, *Appl. Phys. Lett.*, **26**, 318 (1975).
16. M.M. Fejer, J.L. Nightingale, G.A. Magel, and R.L. Byer, *Rev. Sci. Instrum.*, **55**, 1791 (1984).
17. R.S. Feigelson, *J. Cryst. Growth*, **79**, 669 (1986).
18. B.M. Tissue, Lizhu Lu, and W.M. Yen, *J. Luminescence*, **45**, 20 (1990).
19. J.S. Haggerty, Production of Fibers by a Floating Zone Fiber Drawing Technique, NASA, Final Report Contract No. NAS 3-13479, Feb 1971.
20. J.S. Haggerty, W.P. Menashi, and J.F. Wenckus, Apparatus for forming refractory fibers, USP 4,012,213, March 15, 1977.
21. J.K.W. Chen, The Electrical and Optical Properties of Doped Yttrium Aluminum Garnets, PhD Thesis, Department of Materials Science and Engineering, MIT, Cambridge, MA, USA (1994).
22. E.R. Pike, *J. Sci. Instrum.*, **34**, 355 (1957).
23. A.J. Wilson, *J. Sci. Instrum.*, **27**, 321 (1950).
24. C.T. Yen, D.O. Nason, and W.A. Tiller, *J. Mater. Res.*, **7**, 980 (1992).
25. F. Euler, *Acta Cryst.*, **19**, 971 (1965).
26. C.P. Khattak and F.F.T. Wang, BNL Report No. 21638, 1976.
27. J. van den Boomgaard, *Philips Res. Rep.*, **10**, 319 (1955).
28. G. Ziegler, *Z. Metallkunde*, **49**, 491 (1958).
29. T. Kotani, J.K.W. Chen, and H.L. Tuller, to be published.
30. Jos. Kvapil, Jirí. Kvapil, B. Mánek, B. Perner, B.K. Sevastyanov, and V.P. Orekhova, *Krystal Res. and Technnol.*, **17**, 225 (1982).
31. K. Kitamura, S. Kimura, Y. Miyazawa, and Y. Mori, *J. Cryst. Growth*, **62**, 351 (1983).
32. J.H. Sharp, T.P.J. Han, B. Illingworth, and I.S. Ruddock, *J. Crystal Growth*, **131**, 457 (1993).